

Oxygen Stoichiometry and Chemical Expansion of $\text{Ba}_{0.5}\text{Sr}_{0.5}\text{Co}_{0.8}\text{Fe}_{0.2}\text{O}_{3-\delta}$ Measured by in Situ Neutron Diffraction

Steven McIntosh,^{†,‡} Jaap F. Vente,[§] Wim. G. Haije,[§] Dave H. A. Blank,[†] and Henny J. M. Bouwmeester^{*,†}

Inorganic Material Science, Department of Science and Technology, and MESA+ Institute for Nanotechnology, University of Twente, 7500 AE Enschede, The Netherlands, and Energy Research Centre of The Netherlands, 1755 ZG Petten, The Netherlands

Received December 14, 2005

The structure, oxygen stoichiometry, and chemical and thermal expansion of $\text{Ba}_{0.5}\text{Sr}_{0.5}\text{Co}_{0.8}\text{Fe}_{0.2}\text{O}_{3-\delta}$ (BSCF) between 873 and 1173 K and oxygen partial pressures of 1×10^{-3} to 1 atm were determined by in situ neutron diffraction. BSCF has a cubic perovskite structure, space group $Pm\bar{3}m$, across the whole T - $p\text{O}_2$ region investigated. The material is highly oxygen deficient with a maximum oxygen stoichiometry ($3 - \delta$) of 2.339(12) at 873 K and a $p\text{O}_2$ of 1 atm and a minimum of 2.192(15) at 1173 K and a $p\text{O}_2$ of 10^{-3} atm. Good agreement is obtained between oxygen stoichiometry data determined by neutron diffraction and thermogravimetry. In the range covered by the experiments, the thermal and chemical expansion coefficients are $19.0(5)$ – $20.8(6) \times 10^{-6} \text{ K}^{-1}$ and $0.016(2)$ – $0.026(4)$, respectively.

Introduction

Mixed ionic–electronic conducting perovskite oxides $\text{ABO}_{3-\delta}$ are of interest as cathode materials for solid oxide fuel cells (SOFC) and as ceramic membranes (MIEC) for oxygen separation. In these applications, the materials are typically subjected to oxygen partial pressures in the range 1×10^{-5} to 1 atm at temperatures between 973 and 1273 K. The material must exhibit high ionic and electronic conductivity while maintaining structural, chemical, and mechanical stability. The crystal structure and composition are important parameters that influence ion and electron transport, surface kinetics, and mechanical properties.

The oxygen stoichiometry ($3 - \delta$) of these materials decreases with increasing temperature and decreasing oxygen partial pressure $p\text{O}_2$. The oxygen stoichiometry is tuned by selecting more- or less-reducible B site cations or by substituting A site cations with cations of a different charge. $\text{SrCo}_{0.8}\text{Fe}_{0.2}\text{O}_{3-\delta}$ (SCF) is reported to provide one of the largest membrane oxygen fluxes in the series $\text{La}_{1-x}\text{Sr}_x\text{Co}_y\text{Fe}_{1-x-y}\text{O}_{3-\delta}$.^{1–3} However, undesirable ordering of SCF into a brownmillerite type structure, $\text{Sr}_2\text{Co}_{1.6}\text{Fe}_{0.4}\text{O}_5$, has been reported to occur below 1073 K at a $p\text{O}_2$ lower than 0.1 atm.^{1,3–6} This ordered state reduces the oxygen flux, whereas the associated lattice expansion leads to large mechanical

stresses across the membrane.⁷ Recent reports^{8–10} have demonstrated an increase in oxygen flux and an apparent increase in the stability of the cubic perovskite phase upon 50% substitution of Ba for Sr, $\text{Ba}_{0.5}\text{Sr}_{0.5}\text{Co}_{0.8}\text{Fe}_{0.2}\text{O}_{3-\delta}$ (BSCF). In addition to application as a MIEC membrane, BSCF has recently been proposed as a high-performance cathode material for intermediate temperature SOFC.¹¹ Knowledge of the oxygen stoichiometry is essential in understanding the performance of this promising new electrode material.

Lattice expansion in the oxygen-deficient perovskites occurs through two mechanisms. The first is thermal expansion. The second is the chemical expansion that occurs upon a decrease in oxygen stoichiometry, accompanied by reduction of the B site cations with increasing temperature and decreasing $p\text{O}_2$.^{12–17} Chemical expansion is of particular interest for industrial application of MIEC membranes, as chemical expansion on the low- $p\text{O}_2$ side relative to the air

* To whom correspondence should be addressed. E-mail: h.j.m.bouwmeester@utwente.nl.

[†] University of Twente.

[‡] Current address: Department of Chemical Engineering, University of Virginia, Charlottesville, VA 22904-4741

[§] Energy Research Centre of The Netherlands.

- (1) Qiu, L.; Lee, T. H.; Liu, L.-M.; Yang, Y. L.; Jacobson, A. J. *Solid State Ionics* **1995**, *76*, 321.
- (2) Teraoka, Y.; Zhang, H. M.; Okamoto, K.; Yamazoe, N. *Mater. Res. Bull.* **1988**, *23*, 51.
- (3) Kruidhof, H.; Bouwmeester, H. J. M.; Van Doorn, R. H. E.; Burggraaf, A. J. *Solid State Ionics* **1993**, *63–65*, 816.
- (4) Harrison, W. T. A.; Lee, T. H.; Yang, Y. L.; Scarfe, D. P.; Liu, L. M.; Jacobson, A. J. *Mater. Res. Bull.* **1995**, *30*, 621.

- (5) Liu, L. M.; Lee, T. H.; Qiu, L.; Yang, Y. L.; Jacobson, A. J. *Mater. Res. Bull.* **1996**, *31*, 29.
- (6) Grunbaum, N.; Moggi, L.; Prado, F.; Caneiro, A. J. *Solid State Chem.* **2004**, *177*, 2350.
- (7) Pei, S.; Kleefisch, M. S.; Kobylinski, T. P.; Faber, J.; Udovich, C. A.; Zhang-McCoy, V.; Dabrowski, B.; Balachandran, U.; Mieville, R. L.; Poeppel, R. B. *Catal. Lett.* **1994**, *30*, 201.
- (8) Shao, Z.; Xiong, G.; Tong, J.; Dong, H.; Yang, W. *Sep. Purif. Technol.* **2001**, *25*, 419.
- (9) Shao, Z.; Yang, W.; Cong, Y.; Dong, H.; Tong, J.; Xiong, G. *J. Membr. Sci.* **2000**, *172*, 177.
- (10) Vente, J. F.; Haije, W. G.; Rak, Z. S. *J. Membr. Sci.* **2005**, doi: 10.1016/j.memsci.2005.09.046.
- (11) Shao, Z. P.; Haile, S. M. *Nature* **2004**, *431*, 170.
- (12) Armstrong, T. R.; Stevenson, J. W.; Pederson, L. R.; Raney, P. E. *J. Electrochem. Soc.* **1996**, *143*, 2919.
- (13) Larsen, P. H.; Hendriksen, P. V.; Mogensen, M. *J. Therm. Anal. Calorim.* **1997**, *49*, 1263.
- (14) Atkinson, A.; Ramos, T. M. G. *Solid State Ionics* **2000**, *129*, 259.
- (15) Adler, S. B. *J. Am. Ceram. Soc.* **2001**, *84*, 2117.
- (16) Kharton, V. V.; Yaremchenko, A. A.; Patrakeev, M. V.; Naumovich, E. N.; Marques, F. M. B. *J. Eur. Ceram. Soc.* **2003**, *23*, 1417.
- (17) Chen, X. Y.; Yu, J. S.; Adler, S. B. *Chem. Mater.* **2005**, *17*, 4537.

side can lead to large mechanical stresses across the membrane.^{7,14}

The oxygen stoichiometry of perovskite oxides is typically determined by controlled atmosphere thermogravimetric analysis (TGA)^{5,18,19} or coulometric titration.^{20,21} Measurement of oxygen stoichiometry by these techniques requires determination of the starting material oxygen stoichiometry, often calculated by mass change from complete reduction of the material, from which the relative change with temperature and pO_2 is calculated. This relative change is determined very accurately. These measurements are then coupled to separate isobaric expansion measurements to determine the chemical and thermal expansion.^{14,17} In contrast to this, in situ neutron diffraction allows for the simultaneous measurement of the absolute oxygen stoichiometry and crystal structure and allows the possibility of ordering on the oxygen sublattice to be explored. Further, the values are determined independently for each refined structure. From the change of these parameters as a function of temperature and pO_2 , we can derive the total, thermal, and chemical expansion coefficients. The accuracy is determined by the intensity of the incoming neutron beam and counting time per measurement.

Previous in situ neutron diffraction studies on related materials have focused primarily on phase stability at high temperature. Mitchell et al. utilized neutron diffraction to study the phase stability of the multiphase material with overall composition $SrFeCo_{0.5}O_y$ ²² and determined the oxygen content of the perovskite phase $SrFe_{0.8}Co_{0.2}O_{3-\delta}$ ²³ as a function of oxygen partial pressure at 1173 K. Schmidt and Campbell²⁴ determined the oxygen stoichiometry of the cubic perovskite $SrFeO_x$ under air as a function of temperature, modeling the structure as a mixture of the end members of the series, $SrFeO_3$ and $Sr_2Fe_2O_5$. In relation to membrane performance, Li et al.²⁵ examined the stability of $SrFe_{0.2}Co_{0.8}O_{3-\delta}$ membranes under operating conditions. However, neutron diffraction has not previously been utilized to systematically measure the oxygen stoichiometry and cell parameters of oxygen-deficient perovskites as a function of temperature and oxygen partial pressure or to directly measure chemical expansion.

The goals of the present study were 2-fold. First was the determination of the crystal structure and oxygen stoichiometry of BSCF in the $T-pO_2$ window of interest for oxygen separation membranes and SOFC cathodes. Second was the investigation of the expansion behavior of BSCF. In this paper, we report results obtained from neutron-diffraction measurements on BSCF between 973 and 1173 K and pO_2 between 1×10^{-3} and 1 atm.

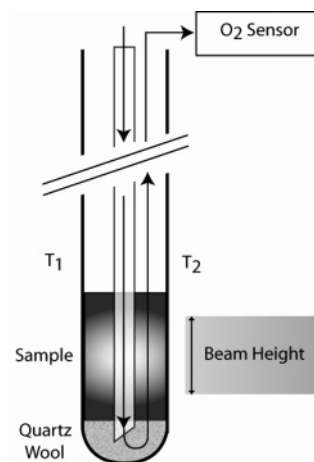


Figure 1. Schematic of sample holder used in neutron experiments. Arrows represent the gas-flow direction and T_1 and T_2 represent thermocouple positions.

Experimental Section

Phase-pure commercial $Ba_{0.5}Sr_{0.5}Co_{0.8}Fe_{0.2}O_{3-\delta}$ (BSCF) powder (Praxair specialty ceramics, Woodinville, WA) was sintered in pellet form at 1373 K for 10 h before being cooled at 1 K/min to room temperature. The pellet was then crushed and the resulting powder sieved to a particle size between 38 and 200 μm . Small particle size is desirable for facilitating rapid equilibration. Neutron-diffraction measurements were carried out on the GEM beamline at the ISIS facility, Rutherford Appleton Laboratories, Chilton, U.K. A room-temperature pattern was collected by placing ~ 2 g of sample in a vanadium can. For the high-temperature measurements, 1.5 g of the sample powder was placed in a quartz sample holder with temperature measured by two thermocouples placed close to the sample but above the incoming neutron beam. Figure 1 is a schematic of the sample holder. The outer tube was a $3/8$ in. o.d. quartz glass with a wall thickness of 0.05 in. and a total length of 20.5 in. Calibrated gas (50 mL/min, STP; CK Gas Products Ltd., Hook, U.K.), in decades of oxygen partial pressure pO_2 from 1×10^{-5} to 1 atm in nitrogen, was supplied through a $1/8$ in. o.d. quartz capillary arranged such that the feed gas passed through the powder sample. The sample holder and inlet and outlet gas lines were sealed outside the furnace hot zone. The holder was placed in a vacuum furnace with the sample exposed to an incoming neutron beam of 4 cm height. The outlet gas pO_2 was continually monitored via a Nernstian sensor (Systech Instruments, Oxford, U.K.).

Ensuring complete equilibration of the sample was of primary concern during these experiments. As discussed above, the sample holder was designed to enable the use of powder samples and to rapidly switch the gas atmosphere. Because of the balance of small particle size, sample holder diameter, and flow rate, we calculated the gas velocity to be above the minimum fluidization velocity of the powder throughout the measurements, placing the bed into the fast fluidization regime.²⁶ Fluidized behavior ensures a well-mixed gas phase, leading to decreased equilibration times. Fluidization was confirmed pre-experiment by observing fluidization of the powder at room temperature and postexperiment by extended discoloration of the quartz tube above the initial sample space. Equilibration at high pO_2 was studied by approaching equilibrium

- (18) Mizusaki, J.; Yoshihiro, M.; Yamauchi, S.; Fueki, K. *J. Solid State Chem.* **1985**, *58*, 257.
 (19) Mizusaki, J.; Mima, Y.; Yamauchi, S.; Fueki, K.; Tagawa, H. *J. Solid State Chem.* **1989**, *80*, 102.
 (20) Lankhorst, M. H. R.; Bouwmeester, H. J. M. *J. Electrochem. Soc.* **1997**, *144*, 1268.
 (21) Lankhorst, M. H. R.; Bouwmeester, H. J. M. *J. Electrochem. Soc.* **1997**, *144*, 1261.
 (22) Mitchell, B. J.; Richardson, J.; Murphy, C. D.; Ma, B.; Balachandran, U.; Hodges, J. P.; Jorgensen, J. D. *J. Eur. Ceram. Soc.* **2002**, *22*, 661.
 (23) Mitchell, B. J.; Rogan, R. C.; Richardson, J.; Ma, B.; Balachandran, U. *Solid State Ionics* **2002**, *146*, 313.
 (24) Schmidt, M.; Campbell, S. J. *J. Phys. Chem. Solids* **2002**, *63*, 2085.

- (25) Li, Y. P.; Maxey, E. R.; Richardson, J. W. *J. Am. Ceram. Soc.* **2005**, *88*, 1244.
 (26) Froment, G. F.; Bischoff, K. B. *Chemical Reactor Analysis and Design*, 2nd ed.; John Wiley & Sons: Hoboken, NJ, 1990.

at 873 K and a pO_2 of 1×10^{-3} atm from a lower and higher pO_2 . Equilibration at low pO_2 was studied by monitoring the outlet pO_2 , lattice parameter, and oxygen stoichiometry as a function of time. Unless otherwise noted, all of the data presented in the following were recorded on fully equilibrated samples where the outlet pO_2 was the same as that of the feed gas.

Data were collected on banks 3, 4, 5, and 6 of the GEM beamline, with d spacing ranges of 0.5–1.85, 0.54–2.705, 0.74–4.1, and 1.3–7.15 Å, respectively. Diffraction patterns were collected during slow heating ramps at 1.33 K/min between 873 and 1273 K while the sample was continually flushed with the calibrated gas mixture and the outlet pO_2 was continuously monitored. The measurement time for each diffraction pattern was dependent on the intensity of the incoming beam and resulted in a temperature spread between 5 and 10 K for each measurement. In the following discussion, data are plotted against the final measurement temperature. The measurements were made in descending pO_2 starting at 1 atm. Before taking measurements at $pO_2 < 0.1$ atm, we oxidized the sample at 1173 K and cooled it to 873 K in 0.1 atm of oxygen. This was to ensure full oxidation of the sample at low temperatures.

Rietveld²⁷ refinements were carried out using the GSAS package.²⁸ An initial fit obtained at room temperature was used as the starting point for the first high-temperature measurement, 873 K in 1 atm of oxygen. Structural refinements were performed sequentially using the structure obtained from the previous refinement as the starting point for the current. The refined parameters were the lattice parameter, isotropic thermal parameters for the A and B cation, anisotropic thermal parameters for the O anion, fractional occupancy of oxygen, scale factors, and σ^{-1} profile parameters for each pattern. The occupancy of the cation sites was fixed according to the known chemical composition, whereas the isotropic thermal parameters of cations on the same site, Ba/Sr and Fe/Co, were constrained to be the same. The oxygen occupancy was refined to determine the oxygen vacancy concentration. The counting time per measurement was optimized to fully analyze the material within the allotted beam time. Estimated standard deviations on the reported values for lattice parameter and oxygen stoichiometry are derived from the fit accuracy for each data point and are typically $\pm 5 \times 10^{-5}$ Å and ± 0.02 , respectively. Longer counting times would lead to a reduction in these errors.²⁹ For the lattice parameters, these were smaller than the symbols used in the figures.

The quartz sample holder contributed a large and convoluted background that could not be adequately removed by subtraction of a background measured on a blank sample holder. As such, shifted Chebyshev functions with 32, 34, 34, and 28 terms were necessary to accurately describe the background of GEM banks 3, 4, 5, and 6, respectively.

Samples for thermogravimetric analysis were prepared by annealing the same BSCF powder at 1273 K for 5 h followed by cooling it in air at 0.5 K/min. The oxygen stoichiometry of this starting material, $3 - \delta = 2.391(5)$, was determined by mass change after reduction in 30% H_2 at 1273 K for 5 h, assuming SrO, BaO, Fe, and Co as products. A known mass of powder ($\sim 20 \mu\text{g}$) was heated at 10 K/min in a platinum sample holder. Calibrated gas (50 mL/min, STP; Praxair Specialty Gases, Oevel Belgium) with pO_2 in decades of oxygen partial pressure from 1 to 1×10^{-3} atm in nitrogen was continually passed through to the sample chamber.

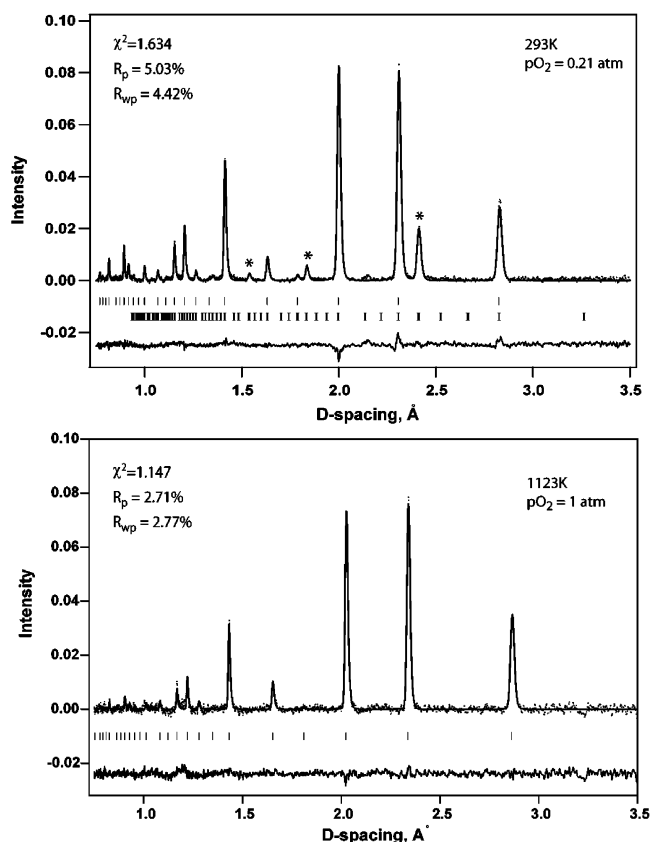


Figure 2. Observed (dots), calculated (top line), and difference (bottom line) powder neutron-diffraction patterns of BSCF at (a) 293 and (b) 1123 K in air and pure oxygen, respectively. Reflection positions where nuclear and/or magnetic Bragg intensities may be observed are marked. The magnetic peaks are marked with an asterisk.

The sample was held at constant temperature, 873–1173 K in steps of 100 K, until constant mass was achieved. The total measurement time at each temperature varied from 4 h at a pO_2 of 1 atm to 10 h at a pO_2 of 1×10^{-3} atm. Equilibration was judged complete when the sample mass varied by less than 0.05% per hour, in line with the instrumental drift. Because of the different gas flow pattern and sample holder design, a direct comparison between these equilibration times and those observed during neutron diffraction was not possible. The mass was corrected for buoyancy by subtracting a blank run. The outlet gas pO_2 was continually monitored via a Nernstian sensor (Systech Instruments, Oxford, U.K.). The total error in the oxygen content determined via TGA, ± 0.007 , was estimated as the sum of the error associated with the initial oxygen content and the 0.05% change in mass per hour during equilibration.

Results

Figure 2 shows two representative neutron diffraction patterns for BSCF. The R_p and R_{wp} values shown on the figure are for the individual pattern where χ^2 is the total for the structural refinement. Figure 2a shows the measured, calculated, and difference patterns collected at room temperature on the air preannealed BSCF sample in a vanadium can. The pattern shows the data collected for bank number 4 covering a d spacing of 0.75–3.5 Å. The background is subtracted from the data. The majority of the peaks could be indexed on a cubic perovskite unit cell with space group $Pm\bar{3}m$. However, three peaks remain unindexed. A G type antiferromagnetic structure, with a refined magnetic moment

(27) Rietveld, H. M. J. *Appl. Crystallogr.* **1969**, *2*, 65.

(28) Larson, A. C.; Von Dreele, R. B. *Los Alamos National Laboratory Report LAUR*; Los Alamos National Laboratory: Los Alamos, NM, 2000; p 86.

(29) McIntosh, S.; Vente, J. F.; Haije, W. G.; Blank, D. H. A.; Bouwmeester, H. J. M. *Solid State Ionics* **2006**, in press.

Table 1. Rietveld Fit Parameters at 1123 K and a pO_2 of 1 Atm^a

atom	site	x	y	z	occupancy	thermal parameters (\AA^2) * 100		
						U_{ISO}	U_{11}	U_{22}
Ba/Sr	1b	0.5	0.5	0.5	1	3.4(1)		
Co/Fe	1a	0	0	0	1	4.3(1)		
O	3c	0.5	0	0	0.757(5)		4.6(2)	5.7(1)
bank	d range (\AA)		R_{wp} (%)	r_p (%)	$D_{\text{W}} - d$			
3	1.3–7.2		3.33	2.72	0.637			
4	0.75–3.50		2.77	2.71	0.810			
5	0.55–2.55		2.91	3.47	0.657			
6	0.49–1.85		4.43	4.84	0.743			
sum	0.49–7.2		3.15	3.45				

$\chi^2(\text{red}) = 1.147$ for 142 variables

^a Parameters: cubic, space group $Pm\bar{3}m$ (221), $a = 4.04661(4)$ \AA , $V = 66.2634(2)$ \AA^3 , $\rho_c = 5.190$ g/cm^3 . Refined parameters: 1 fractional occupancy, 1 cell parameter, 4 thermal parameters, 4 scale factors, 4 profile coefficients in a W. I. F. David function, being a convolution of the Ikeda-Carpenter and pseudo-Voigt functions, 28 + 34 + 34 + 32 background parameters in shifted Chebyshev functions.

of 2.48(1) μ_B per B cation, was required to describe the presence and intensity of the remaining peaks. To the best of our knowledge, this is the first report of magnetic properties in BSCF. The lattice parameter was refined to 3.99350(7) \AA with a refined oxygen stoichiometry ($3 - \delta$) of 2.337(9). This room-temperature oxygen stoichiometry is slightly lower than that of the sample used for thermogravimetry, which may be explained by the different preparation methods. The sample for the thermogravimetric measurements was annealed as a powder, whereas that for the neutron diffraction was annealed as a pellet before crushing. Because of the longer bulk-diffusion lengths and reduced surface area of a pellet, equilibration with air during cooling is slower than for a powder. This prevents full equilibration of the pellet during cooling, resulting in the lower oxygen stoichiometry observed for the neutron-diffraction sample at room temperature. No secondary phases or simple oxides were detected, confirming the phase purity of the starting material.

Figure 2b shows the same d spacing range collected at 1173 K and a pO_2 of 1 atm oxygen. At this elevated temperature, the magnetic reflections disappear, leaving the cubic perovskite structure with space group $Pm\bar{3}m$, a lattice parameter of 4.04661(4) \AA , and oxygen stoichiometry of 2.271(15). The structural parameters and details of the fit for this representative data set are presented in Table 1. All of the high-temperature data presented here could be fitted using the same refinement scheme with quality-of-fit parameters similar to those given in Table 1.

The sample-holder design and small particle size of the sample resulted in relatively fast gas changeover and equilibration kinetics at the higher oxygen pressures measured. This allowed measurements to be taken during temperature ramps instead of at discrete temperature steps. The equilibration kinetics were investigated by two methods.

A neutron-beam outage during the measurement at a pO_2 of 1×10^{-3} atm provided an opportunity to confirm equilibration by approaching the point 873 K and a pO_2 of 1×10^{-3} atm from two different directions. The lattice parameter as a function of time for both approaches is shown in Figure 3. In the first case, the sample was cooled from

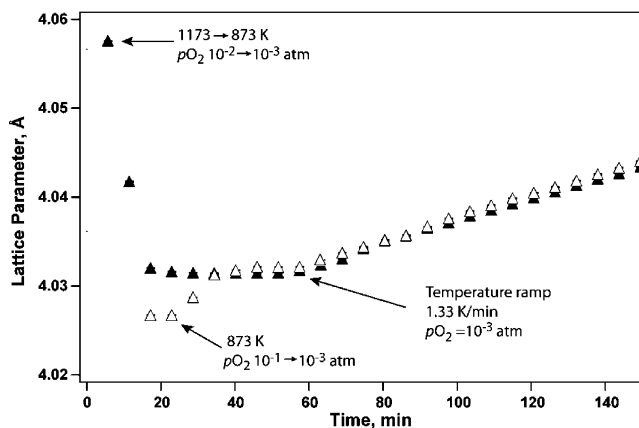


Figure 3. Lattice parameter vs time profiles for two separate approaches to equilibrium at 873 K with a pO_2 of 1×10^{-3} atm. The sample was cooled from 1173 to 873 K as the pO_2 was changed from 1×10^{-2} to 1×10^{-3} atm (\blacktriangle). The pO_2 was changed from 1×10^{-1} to 1×10^{-3} atm at 873 K (\triangle). The initial measurements during the subsequent temperature ramp are also shown.

1173 to 873 K while the pO_2 was simultaneously changed from 1×10^{-2} to 1×10^{-3} atm, resulting in the rapid drop in lattice parameter shown in Figure 3. The lattice parameter and oxygen stoichiometry stabilized to 4.03143(4) \AA and 2.235(12), respectively, within 10 minutes. In the second case, the sample was first equilibrated at 873 K with a pO_2 of 1×10^{-1} atm with a lattice parameter of 4.02672(4) \AA and oxygen stoichiometry of 2.230(12). Introducing the $pO_2 = 1 \times 10^{-3}$ atm gas resulted in a lattice expansion to 4.03211(4) \AA because of reduction of the oxygen stoichiometry to 2.228(12). For both cases, the lattice parameter smoothly increased as the temperature was increased at the start of the measurement ramp. The independence of oxygen stoichiometry and lattice parameter upon approach conditions and the rapid response to changes in gas atmosphere and temperature confirm rapid equilibration of the sample.

The second measure of equilibration kinetics reveals the limitations of measuring at pO_2 less than 1×10^{-3} atm. Figure 4 shows the lattice parameter, oxygen stoichiometry, and outlet oxygen partial pressure vs time for a series of changes of gas atmosphere. The sample was rapidly cooled with a gas-phase pO_2 of 1×10^{-4} atm from 1173 to 873 K in region I. The outlet oxygen partial pressure in region I is below that of the 1×10^{-4} atm feed because of oxygen uptake by the sample. Oxidation occurs upon cooling as the equilibrium oxygen stoichiometry is higher at lower temperature. To oxidize the sample, the gas feed was switched to a pO_2 of 0.1 atm in region II. The sample rapidly oxidizes with the increased pO_2 , as evidenced by the decrease in lattice parameter and increase in oxygen stoichiometry. Re-equilibration occurs within 10 min. Upon a second switch in feed gas to a pO_2 of 1×10^{-5} atm in region III, a slow decay in outlet pO_2 is accompanied by a slow increase in lattice parameter and decrease in oxygen stoichiometry.

The measured lattice parameter as a function of pO_2 and temperature is shown in Figure 5. All of the data were refined to the cubic perovskite structure with random distribution of oxygen vacancies and cations across the associated sublattices. Figure 6 shows the corresponding lattice oxygen stoichiometries determined from the structural fitting of the

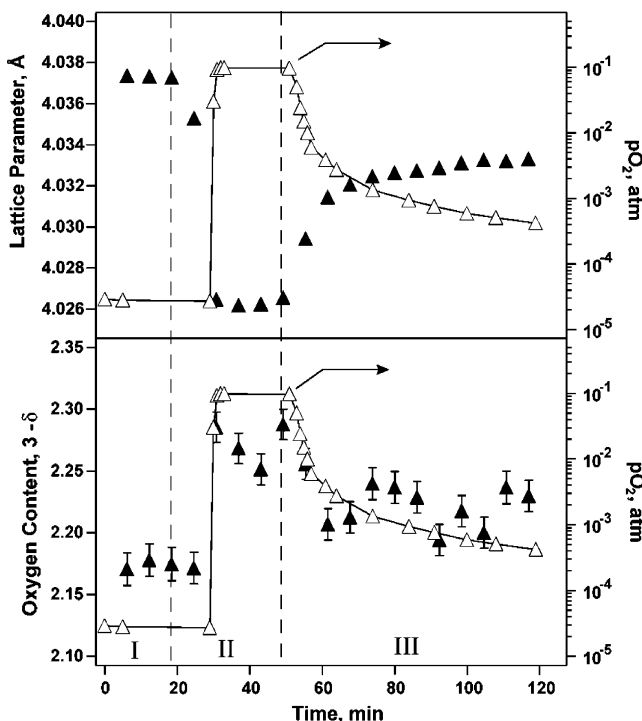


Figure 4. (a) Lattice parameter (▲) and outlet oxygen partial pressure (Δ) vs time and (b) oxygen stoichiometry (▲) and outlet oxygen partial pressure (Δ) vs time (I) following a rapid temperature drop from 1173 to 873 K at a pO_2 of 1×10^{-4} atm (inlet), (II) an inlet gas change to a pO_2 of 0.1 atm, and (III) an inlet gas change to a pO_2 of 10^{-5} atm.

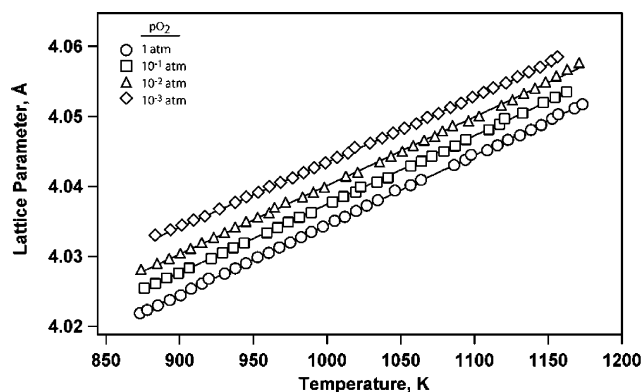


Figure 5. Lattice parameter vs temperature as a function of oxygen partial pressure for $Ba_{0.5}Sr_{0.5}Co_{0.8}Fe_{0.2}O_{3-\delta}$.

neutron-diffraction data. The dashed lines are linear fits and act as a guide to the eye. Note that good agreement is obtained with data determined by thermogravimetry, also shown in Figure 6. Figure 7 depicts the lattice parameter, determined by neutron diffraction, as a function of oxygen deficiency, determined by thermogravimetry, in BSCF at four different temperatures. The dashed lines are again linear fits to the data as a guide to the eye.

Discussion

Ensuring complete equilibration of the sample with the gas environment was a primary concern during these experiments. The rapid response of the sample to changes in temperature and feed pO_2 shown in Figures 3 and 4 are attributed to our sample holder enabling the use of well-mixed, fluidized powder samples. In particular, the close

tracking of outlet pO_2 , lattice parameter, and oxygen stoichiometry shown in Figure 4 is indicative of a well-mixed gas phase in which the oxygen activity of the particle is close to being in equilibrium with the gas. Complete gas mixing within the sample holder allows the oxygen partial pressure of the outlet gas to be assigned to that above the sample. However, some limitations were encountered at low oxygen partial pressures, at which small absolute quantities of oxygen absorbed or released by the sample resulted in large relative changes in the oxygen partial pressure above the sample. This is indicated by the discrepancy between outlet and inlet pO_2 in regions I and III of Figure 4. In region I, the outlet oxygen partial pressure is lower than the 1×10^{-4} atm of the inlet gas, as the sample consumes oxygen upon oxidation. The reverse is true in region III, where the approach to the targeted equilibration of the sample at a pO_2 of 1×10^{-5} atm is frustrated by the release of oxygen from the sample, increasing the gas-phase oxygen content. This subsequent reduction in driving force decreases the equilibration rate. At $pO_2 < 10^{-3}$ atm, times at each temperature would be too long to allow for the collection of reliable data sets. Similar equilibration rates at low pO_2 , also attributable to the release of oxygen from the sample, have been reported in the literature.²³

As shown in Figure 6, the oxygen stoichiometry determined by neutron diffraction is in good agreement with that determined by thermogravimetry. Both methods reveal that the oxygen stoichiometry in BSCF at a given temperature and pO_2 is considerably lower than that reported for related materials.^{5,18,20,30–33} A decreased oxygen stoichiometry in comparison to that observed in the series $La_{1-x}Sr_xCo_{0.8}Fe_{0.2}O_{3-\delta}$ ^{30,32,33} may be expected from charge-compensation arguments. In these compounds, the formation of positively charged oxygen vacancies is induced by substitution of divalent Sr^{2+} onto the La^{3+} site. However, the significantly lower oxygen content of BSCF in comparison to the end member with $x = 1$, $SrCo_{0.8}Fe_{0.2}O_{3-\delta}$ (SCF),^{5,34} is more difficult to reconcile. Earlier, we proposed that the increased basicity of the Ba^{2+} relative to Sr^{2+} would lead to increased stability of the higher oxidation states of the B site cations and, therefore, increased oxygen stoichiometry of BSCF compared to SCF.³⁵ However, the findings presented here prove this incorrect. One suggestion for the reduced oxygen content is the relative size of Ba^{2+} and Sr^{2+} . That is, doping of the larger Ba^{2+} cation onto the Sr^{2+} site in SCF increases the average A–O and B–O bond distances, with a subsequent destabilization of the higher B cation oxidation states.

- (30) Tai, L.-W.; Nasrallah, M. M.; Anderson, H. U.; Sparlin, D. M.; Sehlin, S. R. *Solid State Ionics* **1995**, *76*, 273.
- (31) Mantzavinos, D.; Hartley, A.; Metcalfe, I. S.; Sahibzada, M. *Solid State Ionics* **2000**, *134*, 103.
- (32) Katsuki, M.; Wang, S.; Dokiya, M.; Hashimoto, T. *Solid State Ionics* **2003**, *156*, 453.
- (33) Lankhorst, M. H. R.; ten Elshof, J. E. J. *Solid State Chem.* **1997**, *130*, 302.
- (34) Grunbaum, N.; Moggi, L.; Prado, F.; Caneiro, A. J. *Solid State Chem.* **2004**, *177*, 2350.
- (35) Bouwmeester, H. J. M.; McIntosh, S. *Mixed Ionic–Electronic Conducting Perovskites*; Linderoth, S., Smith, A., Bonanos, N., Hagen, A., Mikkelsen, L., Kammer, K., Lybye, D., Hendriksen, P. V., Poulsen, F. W., Mogensen, M., Wang, W. G., Eds.; Riso National Laboratory: Roskilde, Denmark, 2005; pp 1–14.

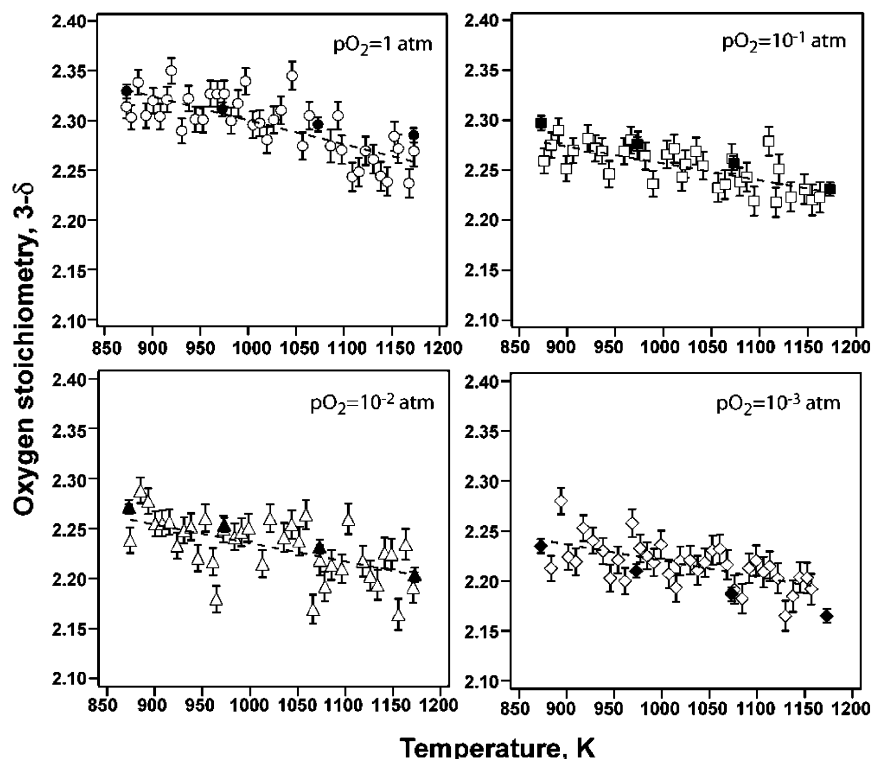


Figure 6. Oxygen stoichiometry vs temperature as a function of oxygen partial pressure for $\text{Ba}_{0.5}\text{Sr}_{0.5}\text{Co}_{0.8}\text{Fe}_{0.2}\text{O}_{3-\delta}$ measured by neutron diffraction (open symbols) and thermogravimetric analysis (closed symbols). Dashed lines are linear fits to the neutron diffraction data.

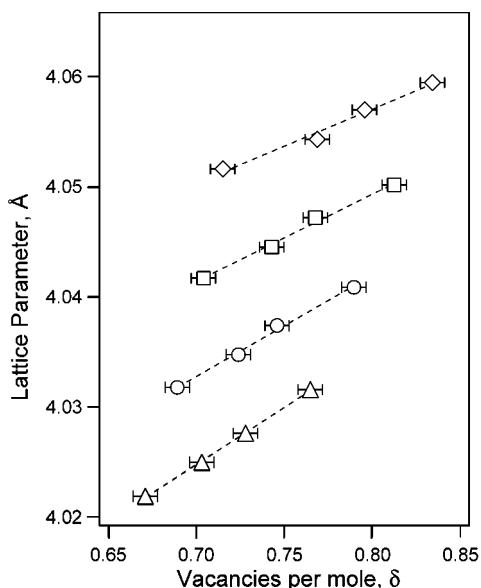


Figure 7. Lattice parameter, from neutron diffraction, vs oxygen deficiency δ , measured by thermogravimetric analysis as a function of temperature for $\text{Ba}_{0.5}\text{Sr}_{0.5}\text{Co}_{0.8}\text{Fe}_{0.2}\text{O}_{3-\delta}$. Dashed lines are linear fits to the data.

The presence of large concentrations of oxygen vacancies may induce vacancy association and ordering in the structure. No evidence for the formation of ordered structures in BSCF was found in the T - $p\text{O}_2$ region studied. This lack of oxygen-vacancy ordering is in contrast to what is found in SCF, which shows ordering into the brownmillerite type structure with ideal composition $\text{Sr}_2\text{Co}_{1.6}\text{Fe}_{0.4}\text{O}_5$, below a $p\text{O}_2$ of 0.1 atm and below 1073 K.^{1,3-5,36} Indeed, the oxygen stoichiometry of BSCF is below that of the vacancy-ordered

brownmillerite type structure under all of the conditions measured in this study. It may be that the presence of mixed A site cations disrupts the uniform A site periodic potential found in SCF, preventing ordering in BSCF. However, the brownmillerite phase has also been observed in compounds with a nonuniform A site periodic potential, such as CaSrMnGaO_5 ³⁷ and $\text{Sr}_{2-x}\text{La}_x\text{Co}_{1.6}\text{Fe}_{0.4}\text{O}_5$.³⁸ An alternative explanation may be that the Ba^{2+} ion is too large to stabilize the transition-metal brownmillerite structure. More research on related compounds is required to draw a definite conclusion.

The chemical and thermal expansion coefficients for BSCF may be extracted from the structural parameters and oxygen stoichiometry presented in Figures 5 and 6. The linear strains associated with the total, chemical, and thermal expansions, respectively, are defined as

$$\epsilon_T = \left. \frac{(a - a_0)}{a_0} \right|_{p\text{O}_2 = \text{constant}} \quad (1)$$

$$\epsilon_c = \left. \frac{(a - a_0)}{a_0} \right|_{T = \text{constant}} \quad (2)$$

$$\epsilon_{\text{Th}} = \left. \frac{(a - a_0)}{a_0} \right|_{\delta = \text{constant}} \quad (3)$$

where a is the lattice parameter and a_0 the lattice parameter at the reference state. For the total expansion, the reference

(36) Grunbaum, N.; Mogni, L.; Prado, F.; Caneiro, A. *J. Solid State Chem.* **2004**, *177*, 2350.

(37) Battle, P. D.; Bell, A. M. T.; Blundell, S. J.; Coldea, A. I.; Gallon, D. J.; Pratt, F. L.; Rosseinsky, M. J.; Steer, C. A. *J. Solid State Chem.* **2002**, *167*, 188.

(38) Prado, F.; Grunbaum, N.; Caneiro, A.; Manthiram, A. *Solid State Ionics* **2004**, *167*, 147.

Table 2. Chemical Expansion Coefficients for $Ba_{0.5}Sr_{0.5}Co_{0.8}Fe_{0.2}O_{3-\delta}$

T (K)	$\Delta a/\Delta\delta$ (Å)	$\epsilon_c = (a - a_0)/a_0$	$\epsilon_c/\Delta\delta$
873	0.103(2)	0.0024(6)	0.026(4)
973	0.091(5)	0.0022(6)	0.022(3)
1073	0.079(4)	0.0018(6)	0.019(2)
1173	0.067(6)	0.0019(6)	0.016(2)

state was 873 K at the pO_2 of interest. For chemical expansion, a_0 was the lattice parameter at a pO_2 of 1 atm and the temperature of interest. For thermal expansion, a_0 was the lattice parameter at 873 K and the δ of interest. The total, chemical, and thermal expansions are defined as $\epsilon_T/\Delta T$, $\epsilon_c/\Delta\delta$, and $\epsilon_{Th}/\Delta T$, respectively.

The total expansion coefficient $\epsilon_T/\Delta T$ was calculated from the data shown in Figure 5 as 24.03(5), 23.19(4), 24.00(5), and $21.49(4) \times 10^{-6} K^{-1}$ for pO_2 of 1, 0.1, 1×10^{-2} , and 1×10^{-3} atm, respectively. These total expansion coefficients are comparable to values reported for similar materials.³⁹ The chemical and thermal expansion coefficients may be extracted from Figure 7, which shows the lattice parameter as a function of oxygen-vacancy concentration at constant temperature. Because of the higher accuracy in the present study for the data of the oxygen-vacancy concentration from thermogravimetric measurements, we used these values to determine the expansion coefficients of BSCF. As noted before, increased counting time during the neutron-diffraction experiments would increase the accuracy of this technique. The calculated thermal expansion coefficients are 20.8(6), 19.8(5), and $19.0(5) \times 10^{-6} K^{-1}$ for $\delta = 0.72, 0.75,$ and 0.80 , respectively. The gradient of the best-fit lines $\Delta a/\Delta\delta$, chemical strain ϵ_c , and chemical expansion coefficients $\epsilon_c/\Delta\delta$ are reported in Table 2. The chemical strain and chemical expansion coefficient are comparable with values reported for similar materials in the literature.¹⁴ A trend of decreasing chemical expansion with increasing temperature may be suggested from these data. This may be due to increased thermal motion within the lattice more easily accommodating the increased vacancy concentration.

This chemical strain leads to a lattice parameter gradient across an operating membrane, which may lead to failure of

the membrane. At 1073 K, the cell parameter increases from 4.04181(5) to 4.05013(1) Å and is associated with a driving force from a pO_2 of 1×10^{-3} to 1 atm. The strain at a single unit-cell dimension would be 0.21%. Real membranes will have a thickness of 10–100 μm . Therefore, it is not anticipated that the chemical stresses will become a limiting factor in the application of BSCF membranes.

Conclusions

BSCF exhibits the cubic perovskite structure across the range of oxygen partial pressure and temperature investigated in this study. The oxygen stoichiometry ($3 - \delta$) determined by Rietveld analyses of neutron-diffraction patterns ranges from 2.192(15) at 1173 K and a pO_2 of 1×10^{-3} atm to 2.339(12) at 873 K and a pO_2 of 1 atm. The oxygen stoichiometry determined from neutron diffraction is in good agreement with that determined by thermogravimetry, which ranges from 2.165(7) to 2.3294(7) at the conditions given above. All oxygen contents are well below the Brownmillerite stoichiometry. The total, thermal, and chemical expansion coefficients were extracted from the refined structural data and the oxygen stoichiometry was determined from thermogravimetry. The total and thermal expansion coefficients of BSCF are 21.49(4)–24.03(5) and 19.0(5)–20.8(6) $\times 10^{-6} K^{-1}$, respectively. The chemical expansion coefficient, the ratio of isothermal chemical strain to change in oxygen stoichiometry, is 0.016(2)–0.026(4). The large concentration of oxygen vacancies and cubic perovskite structure are concordant with the high oxygen fluxes reported for BSCF membranes and the low polarization resistance of BSCF solid-oxide fuel-cell cathodes. In situ neutron diffraction is demonstrated to be a convenient and elegant method for determining oxygen nonstoichiometry and expansion behavior.

Acknowledgment. Financial support for S.M. was provided by the EU Marie Curie Intra-European Fellowship OXYMEM (Contract EIF515272). Further financial support was provided by the Dutch Ministry of Economic Affairs through the EDI program administered by Senter-Novem under Contract EDI03201. The authors are grateful to Paolo Radaelli (ISIS) for experimental assistance.

CM052763X

(39) Kharton, V. V.; Yaremchenko, A. A.; Kovalevsky, A. V.; Viskup, A. P.; Naumovich, E. N.; Kerko, P. F. *J. Membr. Sci.* **1999**, *163*, 307.